

**Atomistic simulation study of the adsorptive separation of
hydrogen sulphide/alkane mixtures on all-silica zeolites**

Tamás Kristóf* and Dóra Bucsai

*Department of Physical Chemistry, Center for Natural Sciences, University of
Pannonia, P.O. Box 1158, H-8210 Veszprém, Hungary*

*Corresponding author.

E-mail address: kristoft@almos.uni-pannon.hu

Atomistic simulation study of the adsorptive separation of hydrogen sulphide/alkane mixtures on all-silica zeolites

The selective separation of the aggressive hydrogen sulphide gas from industrial streams is highly important from environmental and economic aspects. Capture of this substance from industrial gases of light hydrocarbons by all-silica zeolites can be an eco-friendly alternative to the other common absorption/adsorption procedures. The adsorption from binary mixtures of hydrogen sulphide and light alkanes ($\text{H}_2\text{S}/\text{CH}_4$, $\text{H}_2\text{S}/\text{C}_2\text{H}_6$, and $\text{H}_2\text{S}/\text{C}_3\text{H}_8$) on preselected all-silica zeolites was studied by atomistic simulations, using a recently developed force field for hydrogen sulphide. In addition to four experimental all-silica zeolite frameworks (DDR, CHA, ACO, CAS), three of their hypothetical relatives were also drawn into the investigations. The smaller pore size zeolites (ACO, CAS, and particularly one of the hypothetical zeolites) showed remarkable separation performances under real ambient conditions. Among the examined structural details of the studied frameworks, the calculated realistic pore size distributions proved the most appropriate in attempts to unravel the connection between adsorption selectivities and framework structural properties. The investigations were completed by a necessary demonstration of the translational accessibility of the inner cages of the smaller pore size zeolites.

Keywords: adsorption simulation, all-silica zeolite, hydrogen sulphide

1. Introduction

Zeolites are three-dimensional crystalline inorganic polymers consisting of TO_4 tetrahedra, where the tetrahedral centres T are principally Si and Al atoms [1]. The framework atoms usually form rings with 3-12 or more T-O atom pairs (members), and the interconnection of these rings through the bridging O atoms results in well-defined cages and channels (pores) in molecular dimensions. The pores are frequently filled with ions and water molecules that are free to move. High degree of crystallinity, low density and comparatively large free volume are typical of these structures. Zeolites are

applied for catalytic, separation, purification or ion exchange purposes. They can generally tolerate high temperatures, pressures and aggressive chemicals. High-silica zeolites have higher thermal and acid stability and fewer structural defects than low-silica ones. On the other hand, zeolites with low Si/Al ratios accommodate more charge-compensating extraframework cations and tend to be more hydrophilic.

Adsorptive separation of the extremely toxic and corrosive hydrogen sulphide from various industrial gases can be realized by zeolites and a number of works have dealt with this topic [2-9]. As shown by experimental [6,7] and theoretical [8,9] studies, the H₂S loading capacity of hydrophilic low-silica zeolites can be considerably large and, in theory, the adsorption of this polar and acidic substance is more intense on these zeolites than on their high-silica counterparts. However, in zeolites with low Si/Al ratios containing large quantity of extraframework cations, the occurrence of chemical reactions of H₂S can not be excluded [6], and this might cause regeneration difficulties. Furthermore, the presence of water (or other polar substances) should significantly decrease the adsorption of H₂S on these hydrophilic zeolites. As some high-silica zeolites also exhibit reasonable H₂S loading capacities [10], these hydrophobic adsorbents might offer better opportunities to efficiently remove H₂S from, e.g. natural gas extraction streams containing aqueous impurities. Hydrogen sulphide capture from these and other industrial streams of low-carbon hydrocarbons by pure silica zeolites can be an environmental friendly and cost-effective alternative to the widespread amine-based absorption processes. Two recent molecular simulation studies have focused on testing the applicability of the existing pure silica zeolitic frameworks for the task [11,12]; some of the best performing frameworks have already been synthesized in all-silica form and some of them are presently available only with a low to moderate Si/Al ratio. Atomistic simulations with classical force fields may accurately predict the

adsorption properties of such materials and provide molecular insights during the exploration for optimal frameworks. From a merely methodological point of view, a considerable complexity reduction of the search is achieved by confining to all-silica zeolite structures. Until now, however, there is no clear understanding of how the structural details and their interconnections affect precisely the capacity and selectivity of these frameworks, in spite of the huge amount of data accumulated, among others, from the above simulations. It is first of all the selectivity which can depend extremely sensitively on the conditions of the investigation (temperature, pressure, mixture composition) [12], and thus the selection of suitable structures can easily become a very complex problem. On the other hand, novel databases were constructed recently, encompassing millions of hypothetical all-silica zeolitic structures [13-15]. The screening of candidate framework materials in these databases may necessitate machine learning approaches [15-17] with the additional requirement of setting up criteria, which indicate that the synthesis of a certain structure might be possible [17,18].

In this work, we further pursue and characterize by atomistic simulations all-silica zeolite structures favourable for separation of hydrogen sulphide from mixtures with methane and its light homologues, ethane and propane.

2. Materials, methods and computational details

Our primary aim was to study the adsorption of binary $\text{H}_2\text{S}/\text{CH}_4$, $\text{H}_2\text{S}/\text{C}_2\text{H}_6$, and $\text{H}_2\text{S}/\text{C}_3\text{H}_8$ mixtures on four all-silica zeolite frameworks, DDR, CHA, ACO, and CAS, from the IZA-SC (International Zeolite Association - Structure Commission) experimental database [19] (this database identify experimental zeolites with 3-letter codes which is part of the official IUPAC nomenclature). Selection of the frameworks was based partly on earlier simulation results [11,12], partly on the availability of experimental equilibrium adsorption data [10]. The idealized framework data for these

zeolites are listed in Table 1. Zeolite DDR is already applied for gas separation and, of the all-silica IZA frameworks, zeolite CHA is the only one with available experimental equilibrium adsorption data for H₂S [10]. For both zeolites, reasonably good selectivities were predicted with H₂S/light alkane mixtures [11,12]. According to the cited simulation works, zeolites ACO and CAS can also be good candidates for the specified separation purpose. Though zeolite ACO has not been synthesized in all-silica form yet, it has one of the most simple framework structures. Due to the adsorbate sizes, all the selected frameworks were required to possess open channels with larger than 6-membered rings as the limiting pore diameter.

In addition, three further, hypothetical, framework structures were chosen for a detailed investigation from the PCOD database [20], representing one by one the three space groups of the studied IZA structures. Of the countless possibilities, only those structures were selected for which the number of different tetrahedral Si centres is the same as, or only slightly higher than, that of the IZA counterpart (ACO: 1; CAS: 3; DDR: 7; CHA: 1; for the latter two, representing the same space group, the number of different tetrahedral Si centres was kept as small as possible). Then, a computational prescreening was performed, testing these zeolites with an equimolar H₂S/CH₄ gas mixture at 298 K; structures showing low adsorption selectivity in favour of H₂S (or no adsorption at all) were rejected. From the remaining structures, the final hypothetical zeolites were selected, where necessary, by visual comparison with the corresponding IZA counterparts, focusing on the shape of open channels. The structures of the selected hypothetical zeolites mostly fulfil some common energy (lattice energy relative to α -quartz) and interatomic distance criteria of feasibility [18], but the applied criteria for similarity to the above experimental structures ensure a higher possibility that these hypothetical zeolites can be synthesized (for the framework parameters see Table 1).

[INSERT TABLE 1 HERE]

In the simulations with the central H₂S/CH₄ system, rigid all-atom intermolecular potential models were employed, which consist of Lennard-Jones and Coulombic interaction sites (Table 2). The TRAPPE force field [22] was used for the zeolites. For H₂S, a recently developed force field with proven accuracy was adopted [23], in which the interaction sites were located not just at the experimental atomic positions, but two additional massless partial charges were placed in the H-S-H plain, at the opposite side of the sulphur atom (for a more realistic description of the molecular charge distribution). The potential model proposed by Terzyk et al. [24] (which is based on the work of Kaminski et al. [25]) was applied for methane; this potential model has an individual Lennard-Jones energy parameter for the C-H interaction and we slightly modified the energy parameter of the C-C interaction in order to use, as in every other case, the Lorentz-Berthelot combining rule for the unlike interactions. For the other alkanes (ethane and propane), the TRAPPE united-atom potential model [26] was chosen, only allowing flexibility in the CH₃-CH₂-CH₃ angle of propane. The force fields used here for ethane and the zeolites are the same as those of the previous simulation works [11,12] (propane was not inspected in these works).

[INSERT TABLE 2 HERE]

Gas adsorption simulations on the idealized frameworks of the above all-silica zeolites were carried out by the standard grand canonical Monte Carlo methodology using the molecular simulation software package RASPA [27,28]. The composition of the gas phase, the temperature and the total pressure were specified for each simulation and the input chemical potentials of the components were determined from the Peng-

Robinson equation. The simulations involved an equilibration period of at least 20000 cycles and an averaging period of at least 50000 cycles. Each cycle consisted of 50% molecular translation/rotation and 50% configurational-bias insertion/deletion moves [29] (in one cycle, the algorithm tries to move all of the molecules, but the minimum is 20 attempts of move per cycle). Zeolite cages that are accessible by molecular insertion but are inaccessible by translation (physical diffusion) were blocked by placing repulsive dummy atoms at the cage centres; this control was necessary only in the case of zeolite DDR. Standard long-range corrections were applied for the Lennard-Jones interactions and the Coulombic interactions were calculated with the Ewald summation [30] (the cut off radius was 1.4 nm).

The selectivity of H₂S to the investigated alkane was calculated from the equilibrium adsorption loadings (q). The ideal selectivity was defined from the single-component adsorption data as

$$\alpha_{id} = (q_{H_2S} / q_{alkane}) / (p_{H_2S} / p_{alkane}), \quad (1)$$

where p_i is the bulk gas pressure of adsorbate i . For the H₂S/alkane mixtures, the selectivity was determined via the mole fractions of the bulk gas components (y):

$$\alpha = (q_{H_2S} / q_{alkane}) / (y_{H_2S} / y_{alkane}). \quad (2)$$

In addition to selectivity, the equilibrium heat of adsorption, ΔH_{ads} was also calculated. For such potential models, the RASPA software uses the following approximation:

$$\Delta H_{ads} = \langle U_a \rangle - RT, \quad (3)$$

where $\langle U_a \rangle$ is the average potential energy of the adsorbed molecules, T is the temperature and R is the gas constant.

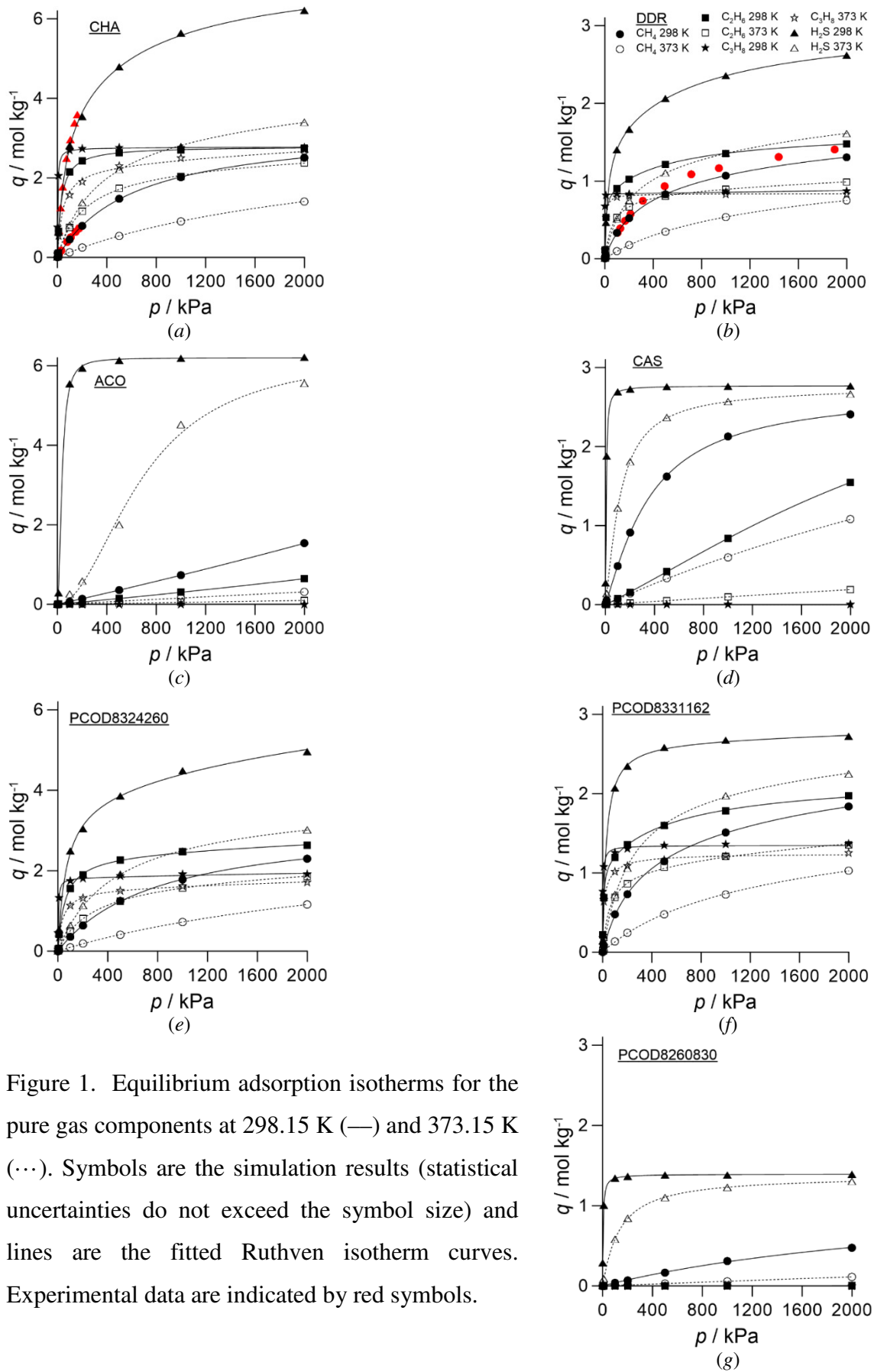
3. Results and discussion

Equilibrium adsorption isotherm data were calculated for the pure gas components at 298.15 and 373.15 K (Figure 1). To draw the isotherm curves, the most simple form of the exponential-series type Ruthven statistical mechanical model equation developed for zeolites [31] was fitted to the simulated data:

$$q = c \cdot \frac{bp + d(bp)^2}{1 + bp + \frac{d}{2}(bp)^2} \quad (4)$$

where b , c , and d are the parameters of the equation. Note that the Langmuir equation is recovered if $d = 0$. In most cases, the maximum loading capacity, provided by parameter c , can simply be estimated from visual inspection of the isotherm curves; with the investigated zeolites, this performance metric turns out to be in the range up to 20 weight % of the adsorbate, with wide variance, for the given gas molecules.

Of the temperature points tested, experimental data are available at 298 K for zeolite CHA with H₂S and CH₄, and for zeolite DDR with CH₄. Using the modified CH₄ potential model, the reproduction of the experimental data is quite good for zeolite CHA and satisfactory for zeolite DDR. It is also seen that the applied new H₂S potential model [23] performs good in the experimental data range: the simulated and experimental data agree very well here.



The predicted equilibrium adsorption loadings are usually significantly higher for H₂S than for the alkanes. The shapes of the curves reveal a Langmuir-like adsorption behaviour, except for H₂S on zeolite ACO, at the higher temperature, where the S shape is likely caused by relatively weaker directed adsorbent-adsorbate interactions acting at low pressures. In the case of the larger pore size zeolites (DDR, CHA, PCOD8324260, and PCOD8331162; see Table 1 and for further details, see later) the degree of adsorption of the larger alkane molecules exceeds that of CH₄ in several simulated points. At low pressures, these zeolites even exhibit higher adsorption loadings with C₃H₈ than with H₂S. The reverse manifestation of this pore size effect can be well recognized from the fact that negligible or no adsorption of C₃H₈ occurred on the smaller pore size zeolites (ACO, CAS, and PCOD8260830; see Table 1). Considering the H₂S uptake capacity, zeolite PCOD8260830 slightly underachieves at higher pressures.

The main results of this work are related to the mixture adsorption predictions shown in Figures 2-4. These figures primarily serve to illustrate the selectivities under real ambient conditions of the studied gas mixtures (for 1% H₂S content, at 298 K and 100 kPa), but results are also presented at a higher temperature, at lower and higher pressures and, as a reference, for equimolar gas mixtures. Statistical uncertainties are not indicated in these complex figures, showing the H₂S coverages in parallel; the statistical errors of the adsorption loadings are usually under 5-6%, but these can reach as high as 10% at extremely low adsorption loadings (we used the standard block average method).

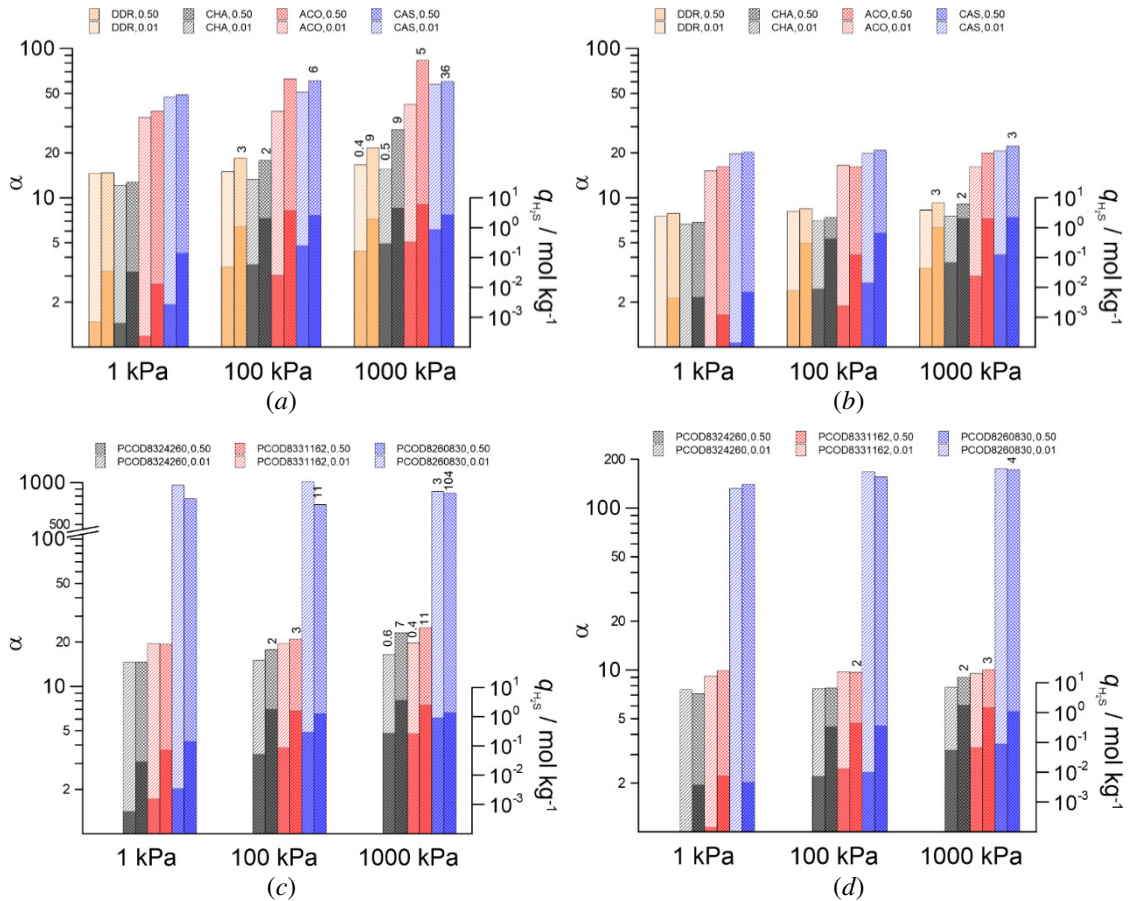


Figure 2. H₂S selectivities (α , crosshatched bars) and H₂S loadings (q , full colour bars) for the equilibrium adsorption from the two kinds of bulk gas mixtures (denoted by the values of 0.50 and 0.01) with CH₄ at 298.15 K (a, c) and 378.15 K (b, d). α/α_{id} data are indicated on the top of the bars.

As a general trend, the selectivity in favour of H₂S increases with pressure and decreases with temperature and no meaningful difference appears between the two gas compositions. The changes are greater as a function of temperature than pressure. Zeolites CHA and DDR behave quite similarly in all cases (as expected). For the other pair of IZA zeolites (ACO and CAS) the similarity in behaviour is noteworthy but more modest. Also in terms of the equilibrium selectivity data, only one of the hypothetical zeolites, PCOD8324260, resembles enough to its IZA counterparts (CHA and DDR).

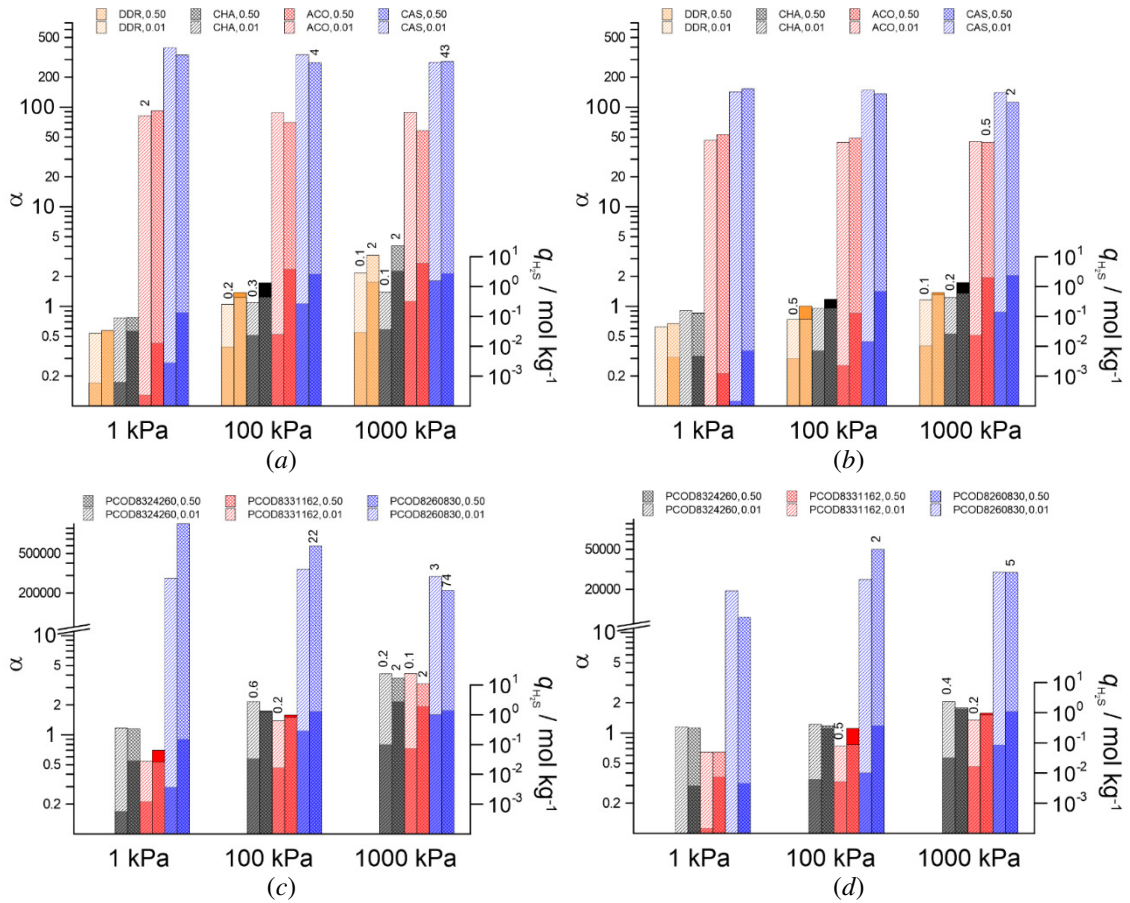


Figure 3. H₂S selectivities (α , crosshatched bars) and H₂S loadings (q , full colour bars) for the equilibrium adsorption from the two kinds of bulk gas mixtures (denoted by the values of 0.50 and 0.01) with C₂H₆ at 298.15 K (a, c) and 378.15 K (b, d). α/α_{id} data are indicated on the top of the bars.

The overall picture that emerges from Figures 3-4 with C₂H₆ and C₃H₈ follows in broad lines the results shown in Figure 2 with CH₄ but the correspondence between the H₂S/C₂H₆ and H₂S/C₃H₈ mixture results is more pronounced.

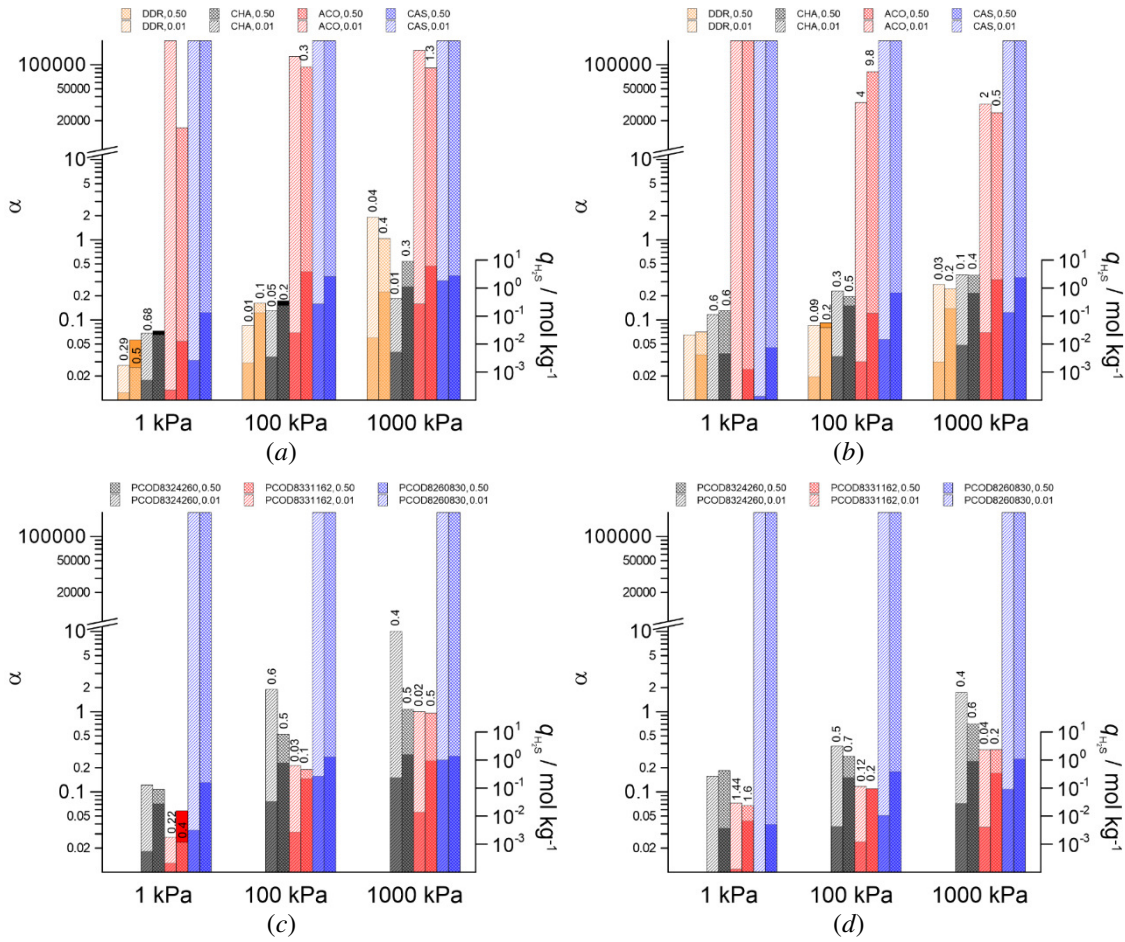


Figure 4. H₂S selectivities (α , crosshatched bars) and H₂S loadings (q , full colour bars) for the equilibrium adsorption from the two kinds of bulk gas mixtures (denoted by the values of 0.50 and 0.01) with C₃H₈ at 298.15 K (a, c) and 378.15 K (b, d). α/α_{id} data are indicated on the top of the bars. (Infinite selectivity is represented by a data bar truncated at the axis end.)

$\alpha = 10$ can be a limiting selectivity below which the applicability of the particular zeolite for such H₂S capture becomes questionable. Considering this limit, zeolites CHA, DDR, PCOD8324260, and PCOD8331162 could only be used for the H₂S/CH₄ gas mixtures and at the lower temperature, 298 K. The low selectivities appearing at lower pressures in the H₂S/C₃H₈ and even in the H₂S/C₂H₆ systems indicate that these larger pore size zeolites prefer the alkanes to H₂S in many cases. On

the other hand, zeolites ACO, CAS, and PCOD8260830 seem promising candidates for future applications. As the figures show, these adsorbents not only exhibit relatively high to extremely high H₂S selectivities but mostly also allow for a comparable degree of adsorption of H₂S to that of zeolite CHA (which is known to have an acceptable measured H₂S uptake capacity [10]). Zeolites ACO, CAS, and PCOD8260830 adsorb propane molecules extremely weakly, or not at all, and the corresponding selectivities become in effect infinite. Although practically applied polar zeolites with low Si/Al ratios often characterized by selectivity values of thousands or ten thousands [9], given other advantages of all-silica zeolites, currently those cases where the selectivities approach to 100 can already be considered very attractive for use.

At 298 K and 1000 kPa, our selectivity data can well be compared with literature results [12] obtained by partially using other potential models. With an equimolar H₂S/CH₄ mixture the present selectivity values are 22, 83, and 60 for zeolites DDR, ACO, and CAS, respectively, while the corresponding literature data with gas mixtures containing somewhat less H₂S are, in the same order, 19, 89, and 28. With an equimolar H₂S/C₂H₆ mixture these values are 3.3, 58, and 287, while the literature data are 3.4, 70, and 79 (in the same order). The general agreement is good, except for zeolite CAS, where the deviations possibly originate from the difference of the applied potential model for H₂S (see above, the potential models for C₂H₆ and the zeolites are the same as those of Ref. [12]). With the H₂S/CH₄ mixtures, the present selectivity data of zeolite CHA at 298 K and 100 kPa agree quite well with other literature results [11].

Mixture selectivity divided by the ideal selectivity, where the pure component adsorption data are taken at the actual partial pressures of the mixture components (see Equation (1)), provides some measure of competition between the gas molecules for the adsorption sites. In this case, at least the initial driving forces of adsorption are equal in

pure-state and in mixture conditions for a particular component. In the course of the adsorption process at higher pressures, however, the component driving forces of mixture adsorption deviate from those of the pure component adsorption and competition is inevitably in place due to the paucity of free space in the zeolite cages. As $\alpha/\alpha_{id} \approx 1$ means no competition, and taking into account the loosely definable nature of such selectivity metrics as well as the uncertainties of determination of the isotherm data (especially at very low pressures), α/α_{id} values are only indicated in Figures 2-4 when $\alpha^{\text{lower}}/\alpha^{\text{higher}}$ is smaller than 2/3 (where α^{lower} and α^{higher} are the lower and higher values in the expression α/α_{id}). Increasing the pressure or decreasing the temperature, these data tend to highlight the difference between systems with the 50% and 1% H₂S gas contents, indicating higher and lower values than 1, respectively. It is somewhat regular that at high adsorption loadings α is smaller than α_{id} at 1% H₂S gas content, where availability of alkane molecules in the gas phase is far prevailing, and it is not surprising that the effect is more prominent with the larger alkanes. However, the low relative selectivities that can be observed on the larger pore size zeolites even at the equimolar gas compositions suggest clear competitive disadvantages of H₂S to the largest alkane. On the other hand, at the equimolar gas compositions there are some relatively high α/α_{id} values for zeolites CAS and PCOD8260830, but this is not specific for zeolite ACO as would otherwise be expected from the primary selectivity data. A comparison of the numerical data showed that the substantial rise in mixture selectivity with respect to the ideal selectivity is always due to the sharp fall in the degree of adsorption of the alkanes. Significant deviations from $\alpha/\alpha_{id} \approx 1$ can have technological importance also in view of the need to reduce losses of alkanes during regeneration of the adsorbent.

The calculated heat of adsorption data for the $\text{H}_2\text{S}/\text{CH}_4$ and $\text{H}_2\text{S}/\text{C}_2\text{H}_6$ mixtures are displayed in Figure 5.

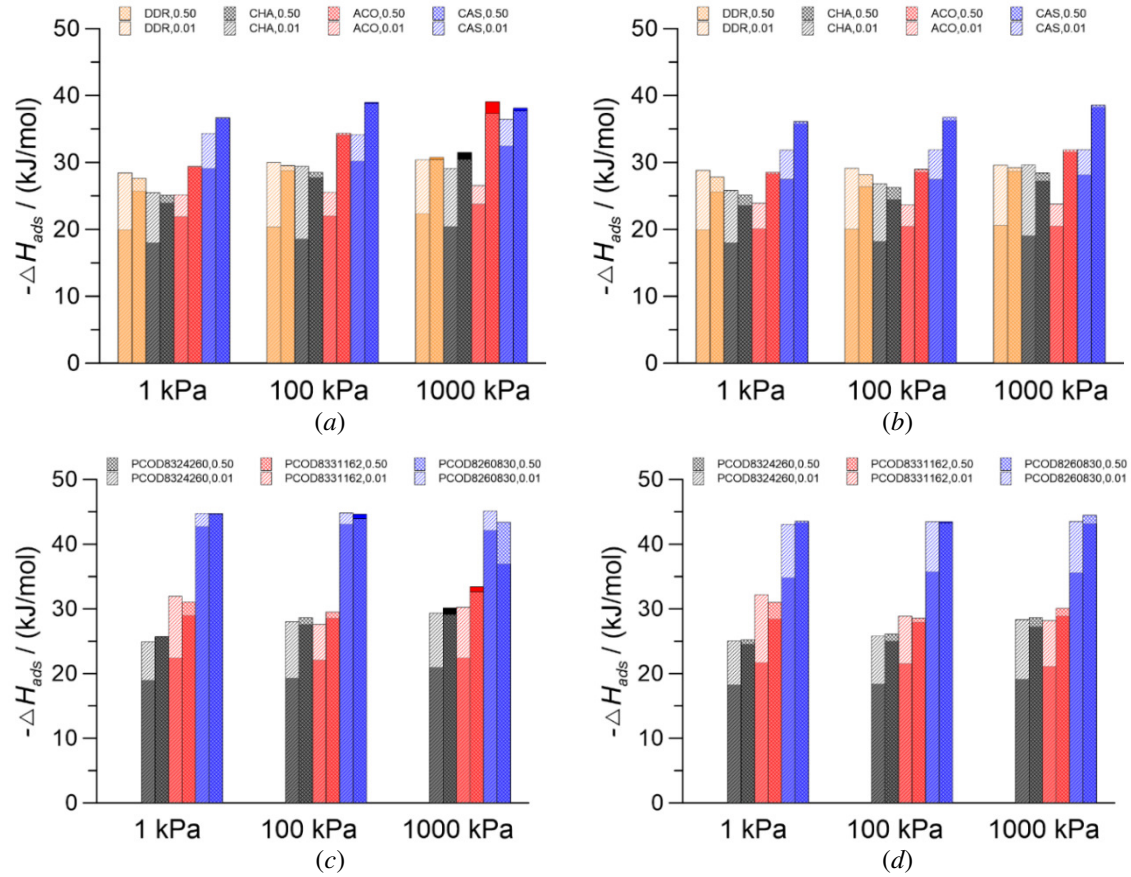


Figure 5. Calculated heat of adsorption data for the equilibrium adsorption from the two kinds of bulk gas mixtures (denoted by the values of 0.50 and 0.01) with CH_4 (full colour bars) and C_2H_6 (crosshatched bars) at 298.15 K (a, c) and 378.15 K (b, d).

With the equimolar gas composition, the $\text{H}_2\text{S}/\text{CH}_4$ dataset nearly match the $\text{H}_2\text{S}/\text{C}_2\text{H}_6$ one, evidently because the adsorption phases contain mainly H_2S . At 1% H_2S content of the bulk gas, the observed higher values for the $\text{H}_2\text{S}/\text{C}_2\text{H}_6$ mixtures arise from the higher adsorption energy of the larger alkane molecule C_2H_6 [32]. The trends of the data apparently reflect the selectivities calculated with the different zeolites. The details of our simulation results show that in all cases the adsorbent-adsorbate

interaction gives the overwhelming contribution to the total heat of adsorption. We also checked this fact in another way, by using the heat of adsorption of the pure substances extrapolated to zero adsorbate coverage (see Table 3) to estimate the mixture data. We found that the adsorption amount-weighted sums of these pure component results satisfactorily approximate the $|\Delta H_{ads}|$ values obtained for the different gas mixtures, with somewhat greater errors at 1000 kPa (at high adsorbate coverages, where the adsorbate-adsorbate interaction can no longer be neglected). We can conclude that the numerical data for the mixtures are, in a first approach, direct consequences of the various adsorbent-adsorbate interaction strengths detected on the different zeolites with pure substances, and zeolites possessing relatively stronger H₂S-framework interactions (i.e., higher $|\Delta H_{ads}|$) obviously show higher selectivities in favour of H₂S. The salient mixture data of zeolite CAS and especially of its hypothetical relative are formally explained by the exceptionally high $|\Delta H_{ads}|$ of pure H₂S on these zeolites, and this departure is consistent with the superior relative selectivities found here. The CAS és PCOD8260830 frameworks have greater atomic densities (see Table 1), which can be a reason for the high $|\Delta H_{ads}|$ values (and for the difference in $|\Delta H_{ads}|$ between the DDR and CHA frameworks, too) as such frameworks enable closer host-guest interactions and closer packing of adsorbates in the binding pores. In practical applications, however, the higher $|\Delta H_{ads}|$ is a disadvantage because it means elevated regeneration (i.e. operating) costs of an adsorption unit.

The correlation between α and $|\Delta H_{ads}|$ was studied in detail in Ref. [11] and established that $|\Delta H_{ads}|$ data not always reflect properly the various selectivity trends with increasing loading of different all-silica zeolites. In our case, the agreement in these trends becomes weaker when going from the H₂S/CH₄ to the H₂S/C₂H₆ and H₂S/C₃H₈ mixtures, partly because the heat of adsorption values of the pure alkanes

become comparable to or exceed those of H₂S. These data and consequently the strengths of adsorbate-framework interactions do not change noticeably with temperature, indicating that at the higher temperature entropic factors must be responsible for the significant reduction in selectivity, disfavoring largely the preferential adsorption of H₂S.

[INSERT TABLE 3 HERE]

In order to get deeper insight into the pore structures, the pore size distributions were approximated in RASPA by calculating the largest spheres for every point as centre in the frameworks that do not overlap with any zeolite atoms [33]. Some elasticity in the frameworks (softness of the atomic spheres) was however taken into account by using 90% of the Lennard-Jones size parameters of the zeolite atoms as the probe distances. Figure 6 shows two important diameter ranges, around 0.3-0.4 and 0.6-0.7 nm and, only for zeolite PCOD8331162, a significantly larger diameter range between 0.8 and 1.0 nm. There are other intense (and broader) peaks below 0.3 nm for zeolites CAS and PCOD8260830 but these are located clearly below the accessibility range by the studied adsorbates. As the method of calculation determines the free space loadable by hard spheres, and not strictly the size of the separate pores in a narrower sense, flat diameter distribution sections with small nonzero probabilities can normally be observed in the distribution curves. In harmony with the literature data of Table 1 [19,21], zeolites ACO, CAS, and PCOD8260830 can be characterized by small pore sizes distributed in not too wide diameter ranges (concerning the numerical differences between the present results and the data of Table 1, note that in the IZA database computation the Si and O atoms of the frameworks are hard spheres with a uniform diameter of 0.27 nm). The area of the lonely peak of zeolite ACO ranged from 0.25 nm

to 0.45 nm covers ~90% of the accessible free space of this zeolite, and those of zeolites CAS and PCOD8260830 cover ~45 and ~50% in the ranges of 0.33-0.49 and 0.27-0.43 nm, respectively. The larger pore size zeolites do not display distinct peaks below 0.5 nm (except for zeolite DDR; its peak around 0.4 nm corresponds to the cages with 5-membered rings as limiting pore entries, and these are inaccessible by translation of the adsorbate molecules). Yet, the areas of the principal peaks up to 0.75 nm cover merely ~45, ~60, and ~50% of the accessible free spaces of zeolites DDR, CHA, and PCOD8324260, respectively (the two separate peaks of zeolite PCOD8331162 together take up ~60%).

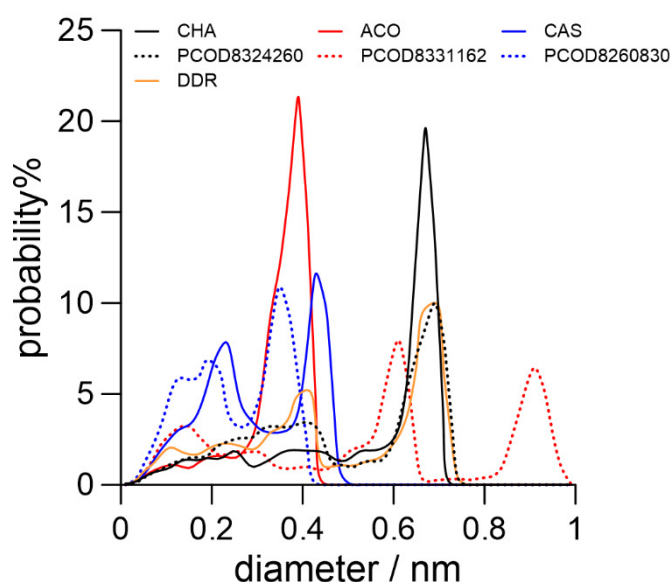


Figure 6. Calculated pore size distributions of the studied frameworks.

Since the small pores in zeolites ACO, CAS, and PCOD8260830 limit the space available for adsorption of the longer C_2H_6 and C_3H_8 molecules, the observed high selectivities seem to be plausible in these cases. As Figures 2-4 show, lower selectivities for the other zeolites generally do not come from significantly lower H_2S coverages, and therefore these are the consequences of the higher degree of C_2H_6 and C_3H_8

sorption. Accordingly, the results with C_2H_6 and C_3H_8 can be considered due to size effects. In view of the vital difference between the curves of zeolite ACO and its hypothetical relative PCOD8331162, these distributions also draw our attention to the very relative importance of the global structural similarities between frameworks; the lower selectivities of the latter is apparently caused by the weaker discriminating power of its larger pores (despite that the latter has greater overall framework density).

Size effects are not trivial in the case of comparable adsorbate sizes, i.e. those of CH_4 and H_2S , and here the stronger H_2S -framework interactions (see $|H_{ads}|$ data in Table 3) can be a reason for the higher selectivities of the smaller pore size zeolites. The stronger H_2S -framework interactions, however, can also be attributed to an indirect size effect, if we consider that in several cases comparable adsorption loadings and accessible free space ratios were detected for different pore size zeolites, and this means that the molecules must be more densely packed in zeolites with smaller pores (enhancing local polar H_2S -framework interactions). The peculiar behaviour of zeolite PCOD8260830 is not immediately seen from the distribution curves, but a closer look at Figure 6 and Table 2 suggest that the critical Lennard-Jones size parameters of the adsorbate models are only slightly below the maximum pore diameter for this zeolite (cf. the feasible diameter of the all-atom model of CH_4 barely fits this maximum diameter). This taut situation of the adsorbates in terms of the possibility of total repulsion by the framework atoms might be responsible for the sharp rise in selectivity with respect to the other zeolites. The fact that very small changes in the zeolitic structure can radically alter the separation behaviour can be well recognized from the sometimes remarkably different separation performances obtained in Ref. [12] with experimental and idealized structures of the same IZA zeolites. These conclusions bring up the possibility that the simulation results are considerably sensitive to the choice of

the force field. To assess the problem, we replaced the all-atom force field for CH₄ by its united-atom counterpart (Table 2), which is known to satisfactorily reproduce experimental pure state and adsorption data of CH₄, also on all-silica zeolites. The adsorption simulations carried out with the equimolar H₂S/CH₄ gas mixture at 298.15 K resulted in very similar adsorption loadings to those calculated by us beforehand for all the studied zeolites, even for zeolite PCOD8260830 and even at higher pressures tested additionally on this zeolite. We could ascertain that small details of difference in force fields with otherwise similar capabilities do not matter, i.e. our results remain in line with expectations that the decisive role belongs to the structural details of the zeolite frameworks.

To distinguish the studied zeolites and to reason their performances, O-Si-O, Si-O-Si, and Si-Si-Si angle and Si-O bond distance distribution analyses [21] were carried out, as well as an identification of preferential binding sites and molecular alignments unique for the different zeolite cages was attempted (based on free energy profiles and atomic density distributions gained from the simulations), but our efforts were not conclusive at this time. The calculated atomic density distributions of a particular adsorbate (three-dimensional histograms of the positions of all atoms of the adsorbate) proved more useful to determine the occupancies of the zeolite cages. Figure 7 shows two examples of these distributions in smaller pore size zeolites collected in the performed grand canonical Monte Carlo simulations. For zeolite ACO a continuous cloud of points can be observed throughout the framework, but for zeolite CAS the density distribution exhibit small gaps between the cages in every direction. It is highly probable that a given type of molecule can diffuse through the framework if such a distribution form a continuous cloud of points at least in one direction. Besides zeolite ACO, it was the case for the larger pore size zeolites. From these results, however, it

was suspected that the adsorbate molecules can not enter the CAS and PCOD8260830 zeolitic cages by translation, and the equilibrium adsorption simulation data are artefacts, owing solely to the random molecular insertion/deletion steps. Therefore, we had to check the reality of these results by specific ‘direct’ simulations.

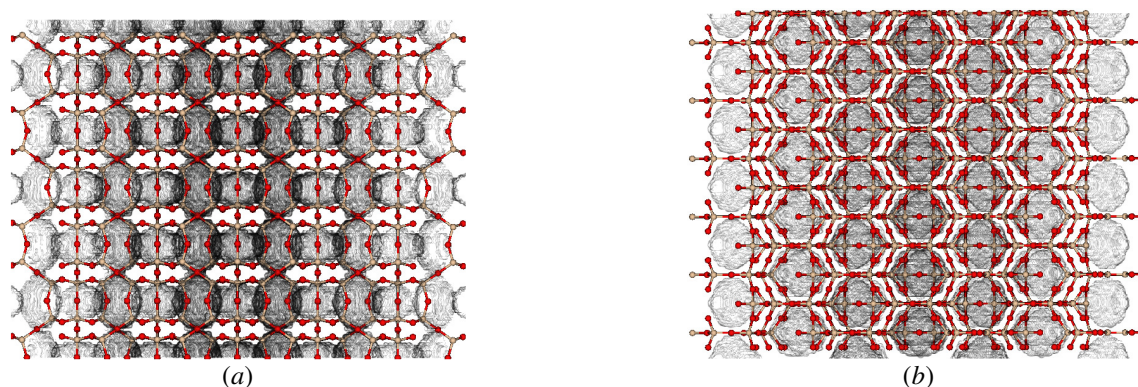


Figure 7. Atomic density distributions for CH₄ obtained in zeolites ACO (a) and CAS (b) from grand canonical Monte Carlo simulations at 298 K and 100 kPa with the equimolar H₂S/CH₄ gas mixture. White areas indicate zero occurrence frequency for the C and H atoms.

It is generally accepted that currently any classical atomistic simulations aiming to produce such equilibrium adsorption data without using artificial molecular insertion/deletion steps are prohibitively long. We experienced the difficulties in very long simulations designed with an explicit gas phase and allowing only translation/rotation moves of the adsorbate molecules in an isothermal molecular dynamics scheme provided in RASPA. The adsorbate gas phases were positioned on one side of the zeolite and initially filled up by random insertion of molecules, while preventing artificially the placement of molecules in the framework (for the whole simulation box, periodic boundary conditions were used). In spite of the generated densely packed (and thus high-pressure) gas phases and the optimally chosen

orientation of the zeolite channels, the gas molecules could generally not overcome the surface resistance of the frameworks and we detected diffusion only into zeolite CHA. The result of such a trial with the very similar zeolite DDR well illustrates the rare-event character of these simulated processes: here we did not observe entering of gas molecules into the inner cages (the cages on the contact surface were cut in half in this case). Then, for a new series of tests, we modified the RASPA code to be able to use it with a constant external force applied in a constricted range of the simulation box. In this way, a depletion zone was created in the original gas phase, on one side of the framework, significantly increasing the pressure acting on the zeolite contact surface on the opposite side. In the new runs, diffusion events were detected with H₂S and CH₄ molecules after several million time steps in the inner cages of each zeolites (as an illustration, see Figure 8). These events were sporadic but clearly identifiable in the case of zeolites CAS and PCOD8260830, which suggests that their channels might also be fully permeable (note also that the largest diameter channels of these zeolites are straight). The third smaller pore size zeolite ACO behaved quite similarly to the larger pore size ones as to the event density. We crosschecked the outcomes of the above tests, starting from the same kind of simulation box but with an empty gas phase and a few adsorbate molecules in the inner cages of the zeolite. In the absence of external field, it was found that the molecules preferred the framework environment all through the performed (technically acceptable) long-term runs. Again, a constant external field, acting across the framework, was needed to drive the molecules into the empty half of the simulation box, even in the case of the larger pore size zeolites. Movies constructed from simulation snapshots gave us insights of how the molecules escaped from zeolites CAS and PCOD8260830, where the process was far more hindered; we found that the greater translational resistance can be attributed to a greater attraction of the framework

atoms of the tighter cages present in these structures, rather than to any sort of visible intercage blockages. In addition, these movies surprisingly showed that, from the two zeolites, the smaller pore size (and more selective) hypothetical framework has weaker translational resistance. That the applied external force did probably not trigger any unrealistic events is supported by the findings with zeolite DDR, where molecules initially inserted into the translationally inaccessible cages with 5-membered limiting rings were ultimately trapped there.

From these tests, it can be stated overall that the penetrability of also the (studied) smaller pore size zeolites is highly probable. However, for all the above reasons, the possibility can not be excluded that real H₂S or CH₄ adsorption experiments with zeolite CAS (or with zeolite PCOD8260830, if synthesizable) will be time-consuming or, despite the simulation predictions, no adsorption is measured at low pressures.

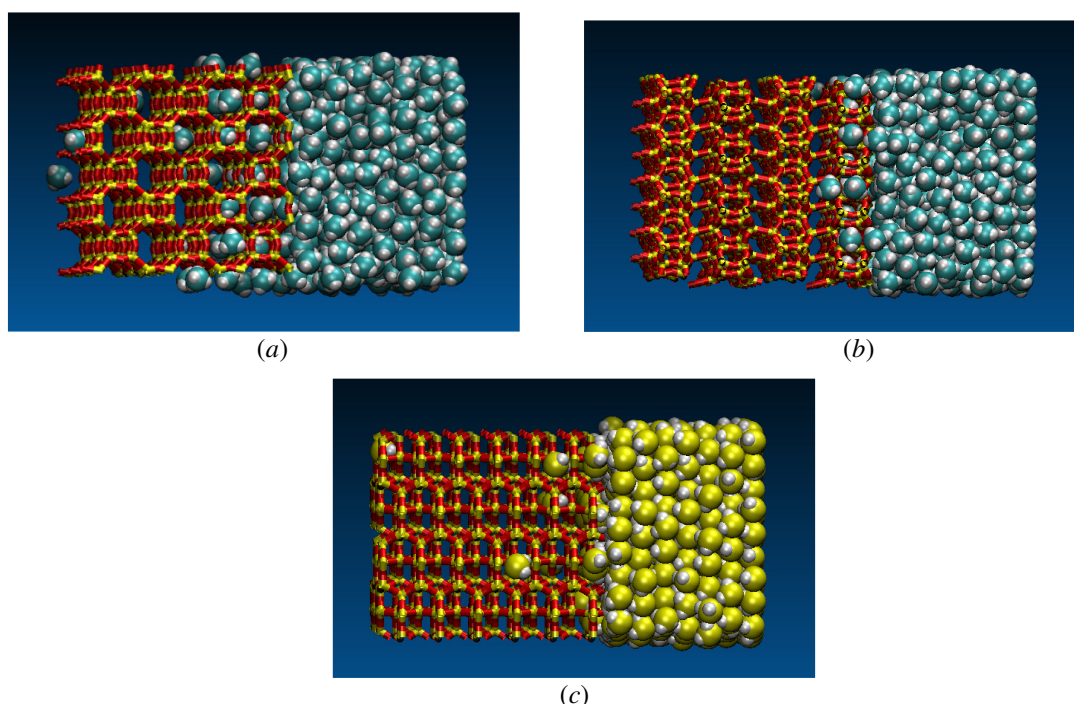


Figure 8. Snapshots from isothermal molecular dynamics simulations at 298 K for illustrating CH₄ and H₂S penetrations into initially empty zeolites ACO (a), PCOD8260830 (b), and CAS (c). An external force of between ~0.4 N and 0.5 nN acting perpendicular to the zeolite contact surface was applied in a ~1 nm wide slab of the opposite end of the condensed phase (the simulation time step was 0.5 fs). (For visual reasons, zeolite frameworks are represented by cylinders for bonds.)

4. Conclusions

We studied the adsorption behaviours of four nanoporous all-silica zeolites (DDR, CHA, ACO, CAS) and three of their hypothetical relatives (PCOD8324260, PCOD8331162, PCOD8260830) with H₂S and light hydrocarbon gases by means of classical atomistic simulations. As we focused on the H₂S capture from industrial streams of CH₄-dominated light hydrocarbons by all-silica zeolites, the H₂S/CH₄ mixture played the central role in our investigations. Accordingly, recent realistic all-atom intermolecular potential models were employed for these components (along with the zeolites) and less detailed potential models were used for the larger alkanes, C₂H₆ and C₃H₈.

H₂S selectivity results were obtained under ambient conditions (at 298 K and 100 kPa) and at other pressures and temperature with 1% and 50% H₂S contents of binary gas mixtures. With the H₂S/CH₄ mixtures, the smaller pore size zeolites (ACO, CAS, PCOD8260830) showed significantly better H₂S separation performances than the other studied zeolites and zeolite PCOD8260830, although possessing a slightly reduced maximum H₂S loading capacity, noticeably outperforms all the others. With the H₂S/C₂H₆ and H₂S/C₃H₈ mixtures, the larger pore size zeolites (DDR, CHA, PCOD8324260, PCOD8331162) turned out to be practically nonselective for H₂S, occasionally even preferring the alkane. Furthermore, as expected from the molecular sizes of the gaseous components, very high (or infinite) H₂S selectivities were observed for the smaller pore size zeolites with the C₂H₆ and C₃H₈ containing mixtures.

Selectivities can have been better predicted from the equilibrium adsorption isotherm data of the pure gas components at lower pressures and at the higher temperature point tested, and when the sizes of the competing components and their mixture mole fractions were similar (i.e. for the H₂S/CH₄ mixture and at the equimolar

gas mixture composition). In comparison with the pure component adsorption data, the significant increase in H₂S selectivity appeared at higher pressures (in particular) is always due to the reduction of the degree of adsorption of the alkanes. Much of the present simulation results for the IZA zeolites are not surprising, since preselected zeolites were drawn into the investigations. IZA zeolites ACO and especially CAS were found promising adsorbents for future use. More interesting still, however, zeolite PCOD8260830, which, if synthesizable, can be exceptionally effective for selective H₂S capture from mixtures with light hydrocarbons.

Among the structural details of the studied frameworks, the occurrence of 8-membered rings as limiting pore openings, which determines the molecules that can be captured by the pores, proved clearly instrumental for the present adsorbate sizes. This in itself simply confirms literature findings [12], however, we refined the picture in this work by calculating realistic pore size distributions and by demonstrating the translational accessibility of the inner cages. We found that the pore size distribution hints at the separation performance but the obtained selectivity trends can not be wholly satisfactorily linked to the dominant pore sizes of the frameworks. For the larger alkane molecules, the selectivity can essentially be ascribed to size effects, but size effects may have a limited impact in the case of CH₄. For the H₂S/CH₄ mixtures, a competing advantage of the polar H₂S molecules is seen from the calculated heat of adsorption data of the pure substances. Consequently, to show a pronounced preference of H₂S over CH₄, the polar character of the Si-O bond must become more effective in the smaller pores of zeolites ACO, CAS, and PCOD8260830.

The revealed sensitivity of selectivity to subtle structural details draws our attention to the role of framework flexibility and defects in real materials, which can be further factors of prediction. The search for all-silica zeolite structures optimal for such

separation purposes is hampered by the scarcity of experimental adsorption data that, among other things, makes testing of the predictive capabilities of these atomistic simulations very difficult. From the strategic point of view, further efforts are needed to identify unique but generic structural details distinctive in terms of selectivity in all-silica zeolites. Currently, it appears highly possible that the analysis of structural diversity of the zeolitic frameworks and the screening of candidate materials will not be based on the classical structure properties (bond distance and angle distributions, ring size, etc.) so much as on more complex geometric descriptors, which capture local atomic structures beyond near-neighbour tetrahedra [34] (and incorporate the ring size as a classical descriptor).

Acknowledgements

Present article was published in the frame of the project GINOP-2.3.2-15-2016-00053 ('Development of engine fuels with high hydrogen content in their molecular structures (contribution to sustainable mobility)'). We gratefully acknowledge the financial support of the National Research, Development and Innovation Office (NKFIH K124353). We thank Zoltán Ható for technical assistance and fruitful discussions.

References

- [1] Auerbach SM, Carrado KA, Dutta PK, editors. Handbook of Zeolite Science and Technology. New York (NY): Marcel Dekker; 2003. ISBN: 0-8247-4020-3
- [2] Shah MS, Tsapatsis M, Siepmann JI. Hydrogen Sulfide Capture: From Absorption in Polar Liquids to Oxide, Zeolite, and Metal-Organic Framework Adsorbents and Membranes. *Chem Rev.* 2017;117:9755-9803.
- [3] Ozekmekci M, Salkic G, Fellah MF. Use of zeolites for the removal of H₂S: A mini-review. *Fuel Proc. Techn.* 2015;139:49-60.
- [4] Liu L, First EL, Hasan MMF, Floudas CA. A multi-scale approach for the discovery of zeolites for hydrogen sulfide removal. *Comp. Chem. Eng.* 2016;91:206-218.
- [5] Georgiadis AG, Charisiou ND, Goula MA. Removal of Hydrogen Sulfide From Various Industrial Gases: A Review of The Most Promising Adsorbing Materials. *Catalysts* 2020;10(5):521.
- [6] Cruz AJ, Pires J, Carvalho AP, Carvalho MB. Physical Adsorption of H₂S Related to the Conservation of Works of Art: The Role of the Pore Structure at Low Relative Pressure. *Adsorption* 2005;11:569-576. DOI: 10.1007/s10450-005-5614-3
- [7] de Oliveira LH, Meneguim JG, Pereira MV, da Silva EA, Grava WM, do Nascimento JF, Arroyo PA. H₂S adsorption on NaY zeolite. *Micropor. Mesopor. Mater.* 2019;284:247-257.
- [8] Cosoli P, Ferrone M, Pricl S, Fermeglia M. Hydrogen sulphide removal from biogas by zeolite adsorption (Part I-II). *Chem. Eng. J.* 2008;145:86-92 and 145:93-99. DOI: 10.1016/j.cej.2008.07.034 & 10.1016/j.cej.2008.08.013
- [9] Kristóf T. Selective removal of hydrogen sulphide from industrial gas mixtures using zeolite NaA, *Hung. J. Ind. Chem.* 2017;45:9-15.

- [10] Maghsoudi H, Soltanieh M, Bozorgzadeh H, Mohamadalizadeh A. Adsorption isotherms of H₂S and CO₂ over CH₄ for the Si-CHA zeolite. *Adsorption* 2013;19:1045-1053.
- [11] Shah MS, Tsapatsis M, Siepmann JI. Monte Carlo Simulations Probing the Adsorptive Separation of Hydrogen Sulfide/Methane Mixtures Using All-Silica Zeolites. *Langmuir* 2015;31:12268-12278.
- [12] Shah MS, Tsapatsis M, Siepmann JI. Identifying Optimal Zeolitic Sorbents for Sweetening of Highly Sour Natural Gas. *Angew. Chem. Int. Ed.* 2016;55:5938-5942.
- [13] Pophale R, Cheeseman PA, Deem MW. A database of new zeolite-like materials, *Phys. Chem. Chem. Phys.* 2011;13:12407-12412.
- [14] Treacy MMJ, Rivin I, Balkovsky E, Randall KH, Foster MD. Enumeration of periodic tetrahedral frameworks. II. Polynodal graphs. *Micropor. Mesopor. Mater.* 2004;74:121-132.
- [15] Helfrecht BA, Semino R, Pireddu G, Auerbach SM, Ceriotti M. A new kind of atlas of zeolite building blocks. *J. Chem. Phys.* 2019;151:154112-1-12.
- [16] Kim B, Lee S, Kim J. Inverse design of porous materials using artificial neural networks. *Sci. Adv.* 2020;6:1-7.
- [17] Muraoka K, Sada Y, Miyazaki D, Chaikittisilp W, Okubo T. Linking synthesis and structure descriptors from a large collection of synthetic records of zeolite materials. *Nature Commun.* 2019;10:4459.
- [18] Li Y, Yu J, Xu R. Criteria for Zeolite Frameworks Realizable for Target Synthesis. *Angew. Chem. Int. Ed.* 2013;52:1673-1677.
- [19] Baerlocher C, McCusker LB. Database of Zeolite Structures. <http://www.iza-structure.org/databases> (April 2020)

- [20] Deem MW. Predicted Crystallography Open Database (PCOD)
<http://www.hypotheticalzeolites.net/database/deem> (April 2020)
- [21] Foster MD, Treacy MMJ. A Database of Hypothetical Zeolite Structures
<http://www.hypotheticalzeolites.net/NEWDATABASE/index.html> (April 2020)
- [22] Shah MS, Tsapatsis M, Siepmann JI. TraPPE-zeo: Transferable Potentials for Phase Equilibria Force Field for All-Silica Zeolites. *J. Phys. Chem. C* 2013;117:24375-24387.
- [23] Cho EH, Lin L. Systematic molecular model development with reliable charge distributions for gaseous adsorption in nanoporous materials. *J. Mater. Chem. A* 2018;6:16029-16042.
- [24] Terzyk AP, Furmaniak S, Gauden PA, Kowalczyk P. Fullerene-intercalated Graphene Nano-containers - Mechanism of Argon Adsorption and High-pressure CH₄ and CO₂ Storage Capacities. *Adsorption Sci.&Techn.* 2009;27:281-296.
- [25] Kaminski G, Duffy EM, Matsui T, Jorgensen WL. Free-energies of hydration and pure liquid properties of hydrocarbons from the OPLS all-atom model. *J. Phys. Chem.* 1994;98:13077-13082.
- [26] Shah MS, Tsapatsis M, Siepmann JI. Transferable potentials for phase equilibria. 1. United-atom description of n-alkanes. *J. Phys. Chem. B* 1998;102:2569-2577.
- [27] Dubbeldam D, Calero S, Ellis DE, Snurr RQ. RASPA: molecular simulation software for adsorption and diffusion in flexible nanoporous materials, *Mol. Sim.* 2016;42:81-101.
- [28] Dubbeldam D, Torres-Knoop A, Walton KS. On the Inner Workings of Monte Carlo Codes, *Mol. Sim.* 2013;39:1253-1292.
- [29] Frenkel D, Smit B. *Understanding Molecular Simulation: From Algorithms to Applications*. San Diego (CA): Academic Press; 2002. ISBN: 0-12-267370-0

- [30] de Leeuw SW, Perram JW, Smith ER. Simulation of electrostatic systems in periodic boundary-conditions. 1. Lattice sums and dielectric-constants. Proc. R. Soc. London, Ser. A 1980;373:27-56.
- [31] Ruthven DM, Goddard M. Sorption and diffusion of C₈ aromatic hydrocarbons in faujasite type zeolites. I. Equilibrium isotherms and separation factors. Zeolites 1986;6:275-282.
- [32] Klimes J, Tew DP. Efficient and accurate description of adsorption in zeolites. J. Chem. Phys. 2019;151:234108-1-10.
- [33] Gelb LD, Gubbins KE. Pore size distributions in porous glasses: a computer simulation study. Langmuir 1999;15:305-308. doi:10.1021/la9808418.
- [34] Helfrecht BA, Semino R, Pireddu G, Auerbach SM, Ceriotti M. A new kind of atlas of zeolite building blocks. J. Chem. Phys. 2019;151:154112.

Table 1. Framework data of the studied zeolites. The maximum diameter of a sphere that can be included in the pores of the zeolite framework [19,21] and the applied simulation box size are also indicated.

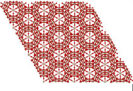
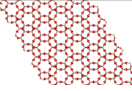
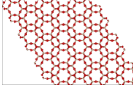
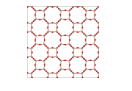
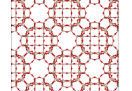
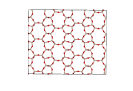
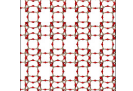
property	DDR	CHA	PCOD 8324260	ACO	PCOD 8331162	CAS	PCOD 8260830
symmetry/ space group	trigonal / 166	trigonal / 166	trigonal / 166	cubic / 229	cubic / 229	ortho- rhombic / 63	ortho- rhombic / 63
framework drawing							
unit cell parameters a, b, c (nm)	1.3795, 1.3795, 4.0750	1.3675, 1.3675, 1.4767	1.3551, 1.3551, 4.3502	0.9905, 0.9905, 0.9905	2.0016, 2.0016, 2.0016	0.5256, 1.4132, 1.7227	1.8829, 0.7443, 1.7107
unit cell parameters α, β, γ (deg)	90, 90, 120	90, 90, 120	90, 90, 120	90, 90, 90	90, 90, 90	90, 90, 90	90, 90, 90
ring sizes	4 5 6 8	4 6 8	4 6 8 12	4 8	4 6 8 10 14 18	5 6 8	4 5 6 8 10
max. sphere diameter (nm)	0.766	0.737	0.754	0.458	0.999	0.505	0.435
framework density (kg/m ³)	1783	1502	1558	1643	1792	1871	1997
simulation box size (unit cells)	3×3×1	3×3×2	3×3×1	3×3×3	2×2×2	6×2×2	2×4×2

Table 2. Lennard-Jones energy (ε) and size parameters (σ) and partial charges (q) for the models used in this work (d is the bond length, k_B is the Boltzmann constant).

interaction site	q / e	$\varepsilon/k_B / \text{K}$	σ / nm	position in the molecule
O	-0.75	53.0	0.330	experimental atomic positions
Si	1.50	22.0	0.230	experimental atomic positions
C (CH ₄)	-0.660	80.0	0.340	$d_{\text{C-H}} = 0.109 \text{ nm}$
H (CH ₄)	0.165	7.901	0.265	H-C-H angle: 109.47°
S (H ₂ S)	-1.152	270.0	0.376	$d_{\text{S-H}} = 0.134 \text{ nm}$, $d_{\text{S-X}} = 0.08764 \text{ nm}$
H (H ₂ S)	0.268	0	0	H-S-H angle: 92.0°
X (H ₂ S)	0.308	0	0	X-S-X angle: 110.0°
CH ₄ (CH ₄)	0	148.0	0.373	-
CH ₃ (C ₂ H ₆ , C ₃ H ₈)	0	98.0	0.375	$d_{\text{C-C}} = 0.154 \text{ nm}$
CH ₂ (C ₂ H ₆ , C ₃ H ₈)	0	46.0	0.395	$d_{\text{C-C}} = 0.154 \text{ nm}$

Table 3. Heat of adsorption of the pure substances extrapolated to zero adsorbate coverage. (Data in parentheses indicate that the extrapolation to zero adsorbate coverage is uncertain due to the very small adsorption amounts (and no adsorption at low pressures).)

$-\Delta H_{ads} / (\text{kJ/mol})$		H ₂ S	CH ₄	C ₂ H ₆	C ₃ H ₈
DDR	298.15 K	26.8	19.1	29.2	37.7
	373.15 K	26.7	19.5	28.9	37.5
CHA	298.15 K	24.8	17.3	27.0	36.7
	373.15 K	24.9	17.6	26.0	33.6
ACO	298.15 K	29.4	19.0	21.7	(11.3)
	373.15 K	28.7	19.0	21.3	(10.9)
CAS	298.15 K	38.2	25.6	25.6	-
	373.15 K	36.7	25.6	25.1	-
PCOD8324260	298.15 K	26.7	17.9	26.1	34.5
	373.15 K	25.6	17.8	25.2	33.0
PCOD8331162	298.15 K	29.9	20.8	29.2	35.1
	373.15 K	28.6	21.0	30.8	35.7
PCOD8260830	298.15 K	45.5	23.6	(14.1)	-
	373.15 K	43.5	23.3	(12.8)	-

Figure captions

Figure 1. Equilibrium adsorption isotherms for the pure gas components at 298.15 K (—) and 373.15 K (···). Symbols are the simulation results (statistical uncertainties do not exceed the symbol size) and lines are the fitted Ruthven isotherm curves.

Experimental data are indicated by red symbols.

Figure 2. H₂S selectivities (α , crosshatched bars) and H₂S loadings (q , full colour bars) for the equilibrium adsorption from the two kinds of bulk gas mixtures (denoted by the values of 0.50 and 0.01) with CH₄ at 298.15 K (*a, c*) and 378.15 K (*b, d*). α/α_{id} data are indicated on the top of the bars.

Figure 3. H₂S selectivities (α , crosshatched bars) and H₂S loadings (q , full colour bars) for the equilibrium adsorption from the two kinds of bulk gas mixtures (denoted by the values of 0.50 and 0.01) with C₂H₆ at 298.15 K (*a, c*) and 378.15 K (*b, d*). α/α_{id} data are indicated on the top of the bars.

Figure 4. H₂S selectivities (α , crosshatched bars) and H₂S loadings (q , full colour bars) for the equilibrium adsorption from the two kinds of bulk gas mixtures (denoted by the values of 0.50 and 0.01) with C₃H₈ at 298.15 K (*a, c*) and 378.15 K (*b, d*). α/α_{id} data are indicated on the top of the bars. (Infinite selectivity is represented by a data bar truncated at the axis end.)

Figure 5. Calculated heat of adsorption data for the equilibrium adsorption from the two kinds of bulk gas mixtures (denoted by the values of 0.50 and 0.01) with CH₄ (full colour bars) and C₂H₆ (crosshatched bars) at 298.15 K (*a, c*) and 378.15 K (*b, d*).

Figure 6. Calculated pore size distributions of the studied frameworks.

Figure 7. Atomic density distributions for CH₄ obtained in zeolites ACO (*a*) and CAS (*b*) from grand canonical Monte Carlo simulations at 298 K and 100 kPa with the equimolar H₂S/CH₄ gas mixture. White areas indicate zero occurrence frequency for the C and H atoms.

Figure 8. Snapshots from isothermal molecular dynamics simulations at 298 K for illustrating CH₄ and H₂S penetrations into initially empty zeolites ACO (*a*), PCOD8260830 (*b*), and CAS (*c*). An external force of between ~0.4-0.5 nN acting

perpendicular to the zeolite contact surface was applied in a ~1 nm wide slab of the opposite end of the condensed phase (the simulation time step was 0.5 fs). (For visual reasons, zeolite frameworks are represented by cylinders for bonds.)